Measurement of electron-impact excitation into the $3p^5 4p$ levels of argon using Fourier-transform spectroscopy

J. Ethan Chilton, John B. Boffard, R. Scott Schappe,* and Chun C. Lin
Department of Physics, University of Wisconsin, Madison, Wisconsin 53706
(Received 4 August 1997)

To experimentally determine electron-impact excitation cross sections with the optical method, it is necessary to measure all transitions out of a level (the *apparent* cross sections), as well as the cascades into the level. In the case of the ten $3p^5 4p$ levels of argon, the emissions to lower levels lie in the visible and near infrared (660–1150 nm) and are hence observable with a monochromator–photomultiplier-tube (PMT) system. A Fourier-transform spectrometer (FTS) allows us to measure the previously uninvestigated cascades that lie in the infrared. For the incident electron energy range between onset and 300 eV, we have measured the apparent cross sections with a monochromator-PMT system, and the cascade cross sections with a weak emission FTS system. The magnitude of both the apparent and cascade cross sections increases with target gas pressure due to radiation trapping effects. By subtracting the cascade contributions from the apparent cross sections, we have determined the direct cross sections and verified that they do not vary with pressure in the 0.5–4-mTorr pressure range considered here. [S1050-2947(98)04201-2]

PACS number(s): 34.80.Dp

I. INTRODUCTION

To understand fully electron excitation of rare-gas systems in laser, lighting, and plasma technologies, accurate values for electron-impact excitation cross sections are required. The optical method provides an experimental approach to determine the rate of electron-impact excitation by measuring the intensity of the emissions from excited atoms. To obtain the direct excitation cross section for a particular level, one must subtract from its total population rate the portion due to cascade radiation from the higher levels that were excited by the incident electrons. These cascade transitions are often in the infrared (IR) and are not readily detectable by photomultiplier tubes (PMT). Solid state devices, such as photodiodes, are sensitive to IR emissions, but with much lower signal-to-noise ratios than that of a PMT operating in the visible spectral region. Achieving a signal-to-noise ratio similar to that of a PMT would require long acquisition times for each spectral line. The Fourier-transform spectrometer (FTS) overcomes this disadvantage by simultaneously observing all transitions within a broad spectral region. Thus for an atom such as argon, with a large number of infrared emissions, we gain over the sequential scanning of a conventional monochromator. The advent of the commercially available weak emission FTS makes possible the use of solid state detectors for infrared detection in electron-impact excitation analysis [1]. In this work, we apply the optical method to the study of electron excitation of argon, using a FTS system to examine previously unmeasured IR transitions.

An energy-level diagram of argon is shown in Fig. 1. The first excited configuration is $3p^5 4s$, and consists of four energy levels with $J=0$, 1, 1, and 2. The wave functions for each level may be expressed as linear combinations of the L-S terms of identical J value. Thus, the two $J=1$ levels of $3p^5 4s$ ($1s_2$ and $1s_4$ in Paschen's notation) contain both the $^1P_1$ and $^3P_1$ components, whereas the $J=0$ and $J=2$ levels ($1s_3$ and $1s_5$ in Paschen's notation) are each represented by a single L-S coupling term, $^3P_0$ and $^3P_2$ respectively, despite the fact that argon does not in general conform to L-S coupling. The apparent cross sections for electron excitation from the $3p^6$ ground level to the two $J=1$ levels have been determined by detecting the emissions from these two levels [2]. Atoms in the $1s_3$ and $1s_5$ levels are metastable and nonradiative. However, by incorporating the technique of

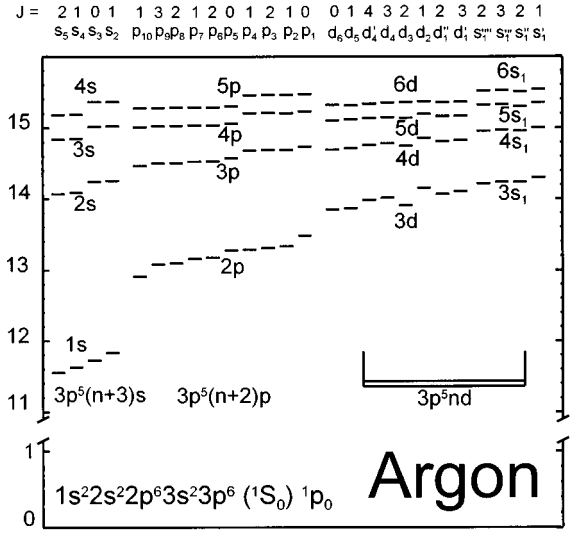

FIG. 1. Argon energy-level diagram (in units of eV). The top of the figure lists the J value followed by the Paschen's notation for each level within the manifold. Translation to configuration notation is provided at the bottom, where n is the numerical prefix for the manifold in Paschen's notation.

*Present address: Department of Physics, Lake Forest College, Lake Forest, IL 60045-2399.

laser-induced fluorescence (LIF), it is possible to measure the apparent excitation cross sections for the $1s_3$ and $1s_5$ metastables using the optical method [3]. The apparent excitation cross sections include the contributions of cascade from higher levels. Most of the cascade radiation into the $1s$ manifold is in the range of 310–920 nm and can be detected easily with a PMT, allowing these cascade corrections to be made.

The next configuration, $3p^5 4p$, contains ten levels, only one of which is a pure L-S level ($^3D_3$, or $2p_9$ in Paschen's notation). Ballou *et al.* [4] have reported the apparent excitation cross sections for all ten levels by measuring the $3p^5 4p \rightarrow 3p^5 4s$ transitions ($2p \rightarrow 1s_2, \ldots, 1s_5$ in Paschen's notation). The majority of the cascade into these levels comes from the $3p^5 5s \rightarrow 3p^5 4p$ ($2s_2, \ldots, 2s_5 \rightarrow 2p$ in Paschen's notation) and $3p^5 3d \rightarrow 3p^5 4p$ ($3d \rightarrow 2p$ and $3s_1 \rightarrow 2p$ in Paschen's notation) transitions. Note that the symbol $3s_1$ refers to four levels within the $3p^5 3d$ configuration, to be distinguished from the $3s_2$, $3s_3$, $3s_4$, and $3s_5$ levels, which arise from the $3p^5 6s$ configuration. These four $3s_1$ levels are denoted by prime superscripts, $3s_1'$, $3s_1''$, etc. Since the $2s \rightarrow 2p$, $3d \rightarrow 2p$, and $3s_1 \rightarrow 2p$ transitions are mostly in the IR, Ballou *et al.* had to resort to theory to estimate the cascade. Because of the complexity of the electronic structure of the excited states of argon, the methods used in the calculations of Ballou *et al.* were not sufficiently accurate to determine direct excitation cross sections.

Using a FTS, we have measured the cross sections for cascade into the $2p$ levels. We can thus determine the direct excitation cross sections based solely on experimental data. Previous experiments [3] indicate that the cross-section data obtained from the intensities of the $2p \rightarrow 1s$ emission lines vary with target pressure even at a few mTorr. Such pressure dependence is often associated with radiation trapping and atom-atom collisional transfer processes populating the excited levels [5]. In the present work we perform measurements across a wide range of pressures (~ 0.1–6 mTorr for the visible transitions, and 0.5–4 mTorr for the IR) and energies (10–300 eV). With the use of the FTS, we have extended the measurements to the IR transitions cascading into the $2p$ levels. In Sec. IV D we will show how these measurements have resolved the source of the pressure dependence.

II. METHOD OF MEASUREMENT

A detailed description of the optical method for measuring electron-impact excitation cross sections has been presented in Refs. [6, 7]; thus only a brief account is given here. Consider a gas of ground-state atoms. An electron beam traverses the gas, exciting some atoms to level i. As they decay to a lower level, j, the resulting fluorescence is detected. Experimentally, we measure the *optical emission cross section* for this transition, which is defined as

$$Q_{ij}^{\mathrm{opt}} \equiv \frac{\Phi_{ij}}{n_0 (I/e)}, \tag{1}$$

where Φ_{ij} is the number of photons per second per unit beam length emitted in the i to j transition, n_0 is the number density of ground-state atoms, I is the electron-beam current, and e the charge of an electron. The sum of all optical emission cross sections from i to the lower levels is termed the *apparent excitation cross section* for the level:

$$Q_i^{\mathrm{app}} = \sum_{j<i} Q_{ij}^{\mathrm{opt}}. \tag{2}$$

A level i may be populated both by direct electron-impact excitation and by higher excited levels cascading into it. Hence, the *direct electron excitation cross section* is obtained from the experimental data by subtracting from the apparent excitation cross section the cascade contribution, which is the sum of the optical cross sections for the transitions into level i from all the levels above it [6], i.e.,

$$Q_i^{\mathrm{dir}} = Q_i^{\mathrm{app}} - \sum_{k>i} Q_{ki}^{\mathrm{opt}}. \tag{3}$$

The $2p$ levels of argon radiatively decay only to the $1s$ levels. Hence, the apparent cross sections of the $2p$ levels can be obtained entirely from the $2p \rightarrow 1s$ optical emission cross sections. The cascade contributions to the $2p$ levels appear to be almost entirely from the $2s$, $3d$, and $3s_1$ manifolds. The experimental task of this work is centered on the measurement of the optical emission cross sections of the $2p \rightarrow 1s$, $2s \rightarrow 2p$, $3d \rightarrow 2p$, and $3s_1 \rightarrow 2p$ transitions at various pressures and electron energies.

III. EXPERIMENTAL APPARATUS

Two separate apparatuses were used in this work. A grating monochromator-PMT system was used to measure all those $2p \rightarrow 1s$ transitions, and the significant $3s \rightarrow 2p$, $4d \rightarrow 2p$, and $4s_1 \rightarrow 2p$ cascade contributions, with wavelengths less than 920 nm. Using a calibrated quartz tungsten halogen lamp, we determined the optical detection efficiency and thus placed the cross sections on an absolute scale using the method described in Ref. [6]. The FTS system was used to measure some of the $2p \rightarrow 1s$ transitions and the entire $2s \rightarrow 2p$, $3d \rightarrow 2p$, and $3s_1 \rightarrow 2p$ manifolds, providing relative cross sections only. Since the FTS and the monochromator-PMT systems overlap in their wavelength range, we use the absolute cross sections for selected emission lines with wavelengths between 850 and 920 nm determined by the monochromator-PMT apparatus to put the FTS measurements on an absolute scale.

A. FTS system

The FTS experimental apparatus is shown in Fig. 2. The vacuum system includes a stainless-steel collision chamber connected to a diffusion pump (700 liters/s) that evacuates the chamber to a base pressure of approximately 2×10^{-8} Torr. During data acquisition, the diffusion pump is valved off, and 99.9995% pure argon gas is admitted to the chamber, filling it to a desired pressure between 0.5 and 4 mTorr. An ion pump connects to the chamber through a leak valve to provide fine adjustment of the pressure during data acquisition, and a getter pump eliminates any extraneous atmospheric gases. A capacitance manometer is used to measure the pressure.

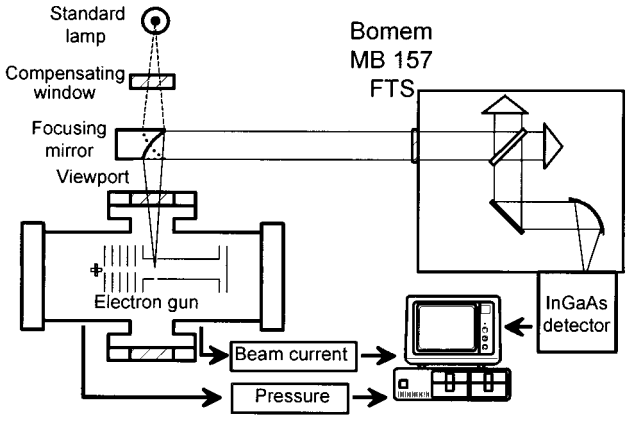

FIG. 2. Layout of the FTS apparatus showing the optics configuration. The focusing mirror can be swiveled 180° to examine the output of a standard lamp.

The electron gun consists of an indirectly heated BaO cathode with four electrostatic focusing and acceleration grids. The gun produces a 200–800-μA beam approximately 3 mm in diameter over an energy range of 10–300 eV. The energy spread of the beam was determined by measuring the Gaussian spread in the onset region of the excitation function, and is estimated to be approximately 0.6 eV. A deep Faraday cup collects the electrons, and a digital multimeter records the current.

A slit in the Faraday cup allows radiation to emerge and pass through a MgF_2 window (transmission $\sim$95% between 0.9 and 5 μm) in the side of the collision chamber. An $f/4$ gold-coated off-axis parabolic mirror collects the light and reflects a collimated beam into a Bomem model MB-157 Fourier-transform weak emission spectrometer. (A comprehensive description of the theory of operation of the FTS may be found in Ref. [8].) A thermoelectrically cooled $In_xGa_{1-x}As$ detector, covering the spectral region between 11 750 and 5900 cm^{-1} (0.85–1.7 μm) at a resolution of 2 cm^{-1}, was used for most measurements. For several longer-wavelength lines in the $3d$ manifold, a liquid-nitrogen-cooled InSb detector, covering 7000–1500 cm^{-1} (1.4–5.8 μm), was used.

B. Monochromator-PMT system

To obtain absolute cross sections, we employ a collision chamber and vacuum system similar to that described in Sec. III A. Details of the operation of this type of apparatus have been published elsewhere [6,9]. The light collected from the excited atoms in the collision region passes through a 1.26-m Czerny-Turner spectrometer and is detected by a PMT with either an $S1$ or a gallium arsenide photocathode. By placing optical stops in the beam path, and comparing the recorded excitation signal with the output of a calibrated standard lamp, we determine absolute cross sections. By placing a polarizing filter in the beam path, it was also possible to determine the degree of polarization of the light emitted from the chamber. Polarization of the excitation signal at all electron energies was found to be too small (generally less than 6%) to require polarization correction [6] in the absolute calibration. For example, a 6% polarization corresponds to a 2% change in the measured cross section, which is much less than the statistical uncertainty of our measurements.

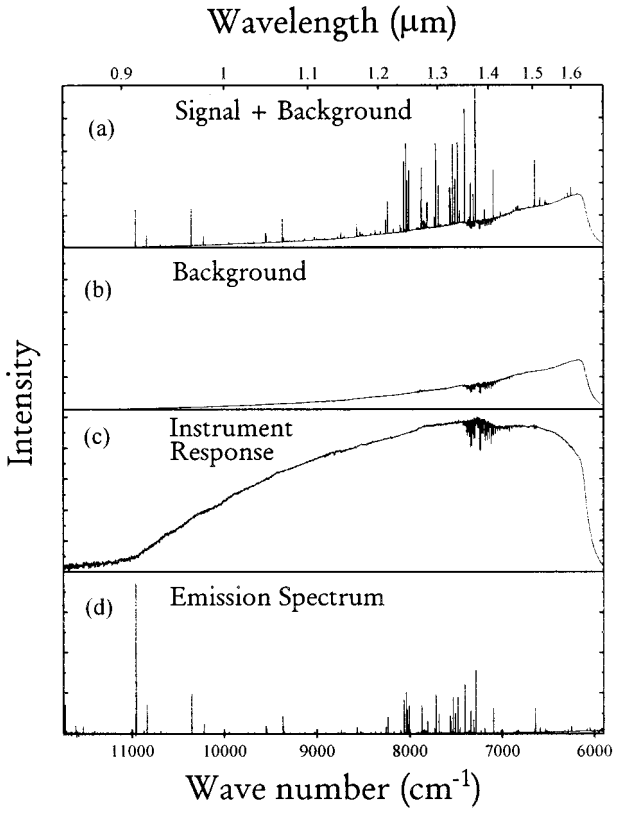

FIG. 3. Measurement of the emission spectrum of 2-mTorr argon at 40 eV. A beam-off background spectrum (b) is subtracted from a beam-on spectrum, with signal+background (a), and the result divided by the instrument response function (c) to yield a wavelength-corrected spectrum (d).

C. FTS data acquisition

Acquisition of emission data with the FTS is a straightforward process. Once the collision chamber is brought to the desired pressure and the accelerating voltage selected, the FTS records 150 scans of the radiation emitted from the collision chamber. One of the advantages of the FTS is that it acquires data on all transitions within its wavelength range during each scan. The resultant spectrum shows peaks due to the excited argon atoms, superposed on a blackbody emission curve due to light scattered from the hot cathode of the electron gun (see Fig. 3). A background spectrum, taken with an electron beam energy below the onset of excitation, is then subtracted, yielding the true excitation signal. The spectrum is corrected for both the detector efficiency and the transmittance factors of the optical system by rotating the parabolic mirror 180° and measuring the signal from a calibrated blackbody source (a quartz tungsten halogen lamp for the $In_xGa_{1-x}As$ detector, and a ceramic element IR blackbody for the InSb detector), as shown in Fig. 2. A MgF_2 window, identical to that on the collision chamber, is placed in the beam path for compensation, and a number of scans acquired. Dividing the resulting spectrum by the known blackbody emission spectrum yields the instrument response. The raw argon excitation spectrum is then divided by the

TABLE I. Wavelengths (in nm) for all allowed $2p \rightarrow 1s$ transitions.

	$2p_1$	$2p_2$	$2p_3$	$2p_4$	$2p_5$	$2p_6$	$2p_7$	$2p_8$	$2p_9$	$2p_{10}$
$1s_2$	750.4	826.5	840.8	852.1	858.1	922.4	935.4	978.5		1148.8
$1s_3$		772.4		794.8			866.8			1047.0
$1s_4$	667.7	727.3	738.4	747.1	751.5	800.6	810.4	842.5		965.8
$1s_5$		696.5	706.7	714.7		763.5	772.4	801.5	811.5	912.3

instrument response function to produce the wavelength-corrected excitation spectrum. Fig. 3 illustrates this process.

Each transition appears as a spectral peak with a line shape arising from the apodization function in the Fourier-transform calculation [8]. The area of the peak represents the number of photons collected from that transition, and is thus proportional to the photon flux. In our wavelength range, we have verified that the height of each peak is directly proportional to the area. Dividing the height by the pressure and electron current produces a set of relative cross sections. Absolute values are assigned to each transition by normalizing the FTS value for the $2p_{10} \rightarrow 1s_5$ (912.3 nm) to that measured absolutely with the monochromator-PMT system.

IV. RESULTS AND DISCUSSION

A. Pressure dependence of the apparent excitation cross sections

Absolute optical emission cross sections for the $2p \rightarrow 1s$ transitions with $\lambda < 920$ nm were measured with the monochromator-PMT system at a gas pressure of 1 mTorr and at incident electron energies corresponding to maximum cross section (~ 20 eV), and at 40 and 100 eV. As noted earlier, the polarization correction is negligible. In addition, we measured the shape of the excitation functions for the ten $2p$ levels between 10 and 300 eV at pressures of 1 and 3 mTorr. Finally, for each of the $2p$ levels, measurements were made of the relative cross section versus pressure at three energies (20, 40, and 100 eV) for pressures between about 100 μTorr and 6 mTorr. Given the excitation functions and pressure dependence curves, along with the set of absolute measurements, it is possible to obtain absolute values for the $2p$ optical cross sections at any pressure and energy. The wavelengths of all the $2p \rightarrow 1s$ transitions are shown in Table I.

The FTS system was used to measure the cross sections of the six IR $2p \rightarrow 1s$ transitions with $\lambda > 920$ nm, and the $2s$ and $3d$ transitions cascading into the $2p$ levels at 20, 40, and 100 eV and five different pressures (0.5, 1, 2, 3, and 4 mTorr). At each energy, five separate data runs of 150 scans each were averaged and the one-sigma deviation calculated. The shapes of the excitation functions were recorded at 1 and 3 mTorr between 10 and 300 eV. Summation of the optical emission cross sections for the appropriate $2p \rightarrow 1s$ transitions, as defined by Eq. (2), yields the apparent excitation cross sections for the $2p$ levels.

To illustrate the effect of pressure, we show in Fig. 4 plots of optical emission cross sections versus pressure for transitions from $2p_5$ ($J=0$), $2p_7$ ($J=1$), $2p_6$ ($J=2$), and $2p_9$ ($J=3$). The pressure dependence for transitions from $2p$ levels of the same J is qualitatively similar. Since the optical emission cross section Q_{ij}^{opt} is equal to the apparent excitation cross section Q_{ij}^{app} times the optical branching ratio Γ_{ij}, the curves in Fig. 4 also give the observed pressure dependence of the apparent excitation cross sections, provided we rescale each vertical axis by the appropriate branching ratio. Of special interest is that the $J=3$ level exhibits much less pressure dependence than all the other $2p$ members. This will be addressed later.

B. Measurement of the cascade cross sections

The largest portion of the cascade into the $2p$ levels comes from the $2s$, $3d$, and $3s_1$ levels. These cascading levels, along with their J values, are shown in Fig. 1. Most of these cascading lines are in the wavelength range of 0.85–1.6 μm, requiring their emission cross sections to be measured with the FTS system ($In_xGa_{1-x}As$ detector module). For transitions with $\lambda > 1.6$ μm, we determine their cross sections with the use of the Einstein A coefficients [10,11] or branching ratios [12] and the measured cross sections for transitions with the same upper level [6]. For instance, from our measured cross section of the $3d_3 \rightarrow 2p_{10}$ line ($\lambda = 1.244$ μm) we can obtain the cross section of the $3d_3 \rightarrow 2p_6$ line ($\lambda = 1.695$ μm) from the relation

$$Q^{\mathrm{opt}}(3d_3 \rightarrow 2p_6) = \left[\frac{A(3d_3 \rightarrow 2p_6)}{A(3d_3 \rightarrow 2p_{10})}\right] Q^{\mathrm{opt}}(3d_3 \rightarrow 2p_{10}). \tag{4}$$

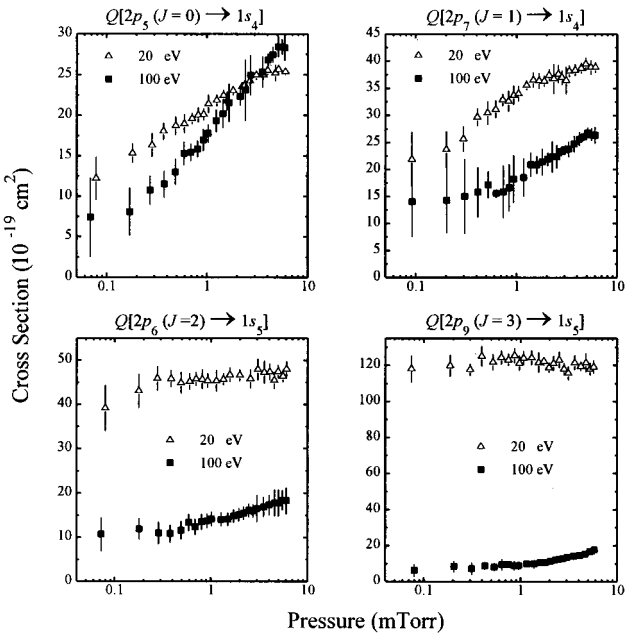

FIG. 4. Optical emission cross section vs pressure at 20 and 100 eV. Error bars are purely statistical.

TABLE II. Optical cross sections for individual cascade transitions at 40 eV and 1 mTorr in units of 10^{-19} cm^2. The initial states are listed in the first column, final states in the first row. Blank entries represent forbidden transitions. A zero entry represents a transition too small to be observed (generally $<4\times10^{-21}$ cm^2). Uncertainties on the individual cross sections are statistical only. Uncertainties on the total cascades represent statistical and systematic errors.

		$2p_1$ ($J=0$)	$2p_2$ ($J=1$)	$2p_3$ ($J=2$)	$2p_4$ ($J=1$)	$2p_5$ ($J=0$)	$2p_6$ ($J=2$)	$2p_7$ ($J=1$)	$2p_8$ ($J=2$)	$2p_9$ ($J=3$)	$2p_{10}$ ($J=1$)
$2s_2$	($J=1$)	1.1±0.2	0.81±0.10	3.7±0.5	0.60±0.08	0.32±0.09	0.64±0.08	0	0.06±0.01		0.40±0.22
$2s_3$	($J=0$)		0.65±0.13		1.2±0.3			0.16±0.06			0.31±0.22
$2s_4$	($J=1$)	0.08±0.02	0	0.04±0.04	0.20±0.06	0.92±0.14	1.5±0.2	2.6±0.3	4.0±0.5		1.0±0.2
$2s_5$	($J=2$)		0	0.19±0.13	0		0.70±0.17	0	0.98±0.15	5.9±0.9	3.6±0.7
$3d_1'$	($J=3$)			0			5.9±0.9		0.69±0.12	1.5±0.2	
$3d_1''$	($J=2$)		0.53±0.16	0	0		0.82±0.11	4.6±0.7	2.4±0.4	0.21±0.12	0
$3d_2$	($J=1$)	0.43±0.13	0.41±0.21	0	0.26±0.10	4.5±0.9	0	5.7±1.0	0.41±0.06		0
$3d_3$	($J=2$)		0.26±0.08	0.99±0.30	0.15±0.04		5.8±1.8	1.1±0.2	0.43±0.07	0	9.1±1.5
$3d_4$	($J=3$)			0			0.21±0.04		11±1	0	
$3d_4'$	($J=4$)									13±2	
$3d_5$	($J=1$)	0	0.19±0.06	0.22±0.07	0.04±0.01	0.44±0.13	1.3±0.4	0.23±0.07	0		7.3±1.2
$3d_6$	($J=0$)		0.46±0.14		0.05±0.02			0			3.5±0.6
$3s_1'$	($J=1$)	4.6±0.8	4.6±0.8	0.34±0.19	3.0±0.5	0.51±0.14	0.25±0.05	0.12±0.06	0		0
$3s_1''$	($J=2$)		2.8±0.5	0.24±0.10	0		1.3±0.2	0.18±0.05	0.28±0.07	0	0
$3s_1'''$	($J=3$)			7.5±0.9			0		0	0.26±0.14	
$3s_1''''$	($J=2$)		0	0.76±0.19	4.5±0.8		0	0	0.36±0.08	0	0
	Total	6.3±1.5	11±2	14±3	10±2	6.7±1.6	18±4	15±3	20±4	21±5	25±2

We have tried to measure directly the cross sections for the cascading lines with $\lambda>1.6$ μm by using an InSb detector module, which covers the wavelength range of 1.4–5.8 μm. However, the InSb detector has a much lower sensitivity than the $In_xGa_{1-x}As$ detector (its D^* value is about a factor of 50 lower), so that many of these transitions were unobservable. By examining the noise amplitude in the spectral region of the transition, we can place an upper bound on the transition. In each case, this upper bound is consistent with the value given in Eq. (4). Furthermore, in all cases these long-wavelength transitions comprise less than 2% of the total cascade contribution to their respective levels.

The next series of cascades into the $2p$ levels are from the levels in the $3p^5 6s$ ($3s_2,\ldots,3s_5$ in Paschen's notation) and $3p^5 4d$ ($4d$ and $4s_1$ in Paschen's notation) configurations with wavelengths in the PMT detector region. Ballou *et al.* [4] have measured cross sections for emission from nine of the twelve levels of $3p^5 4d$, but transitions from the other three levels were too weak to measure. Ballou *et al.* also showed excitation functions for the $3p^5 6s$ levels but gave no magnitude for the cross sections. We have measured the cross sections for the $3p^5 6s\rightarrow 3p^5 4p$ and $3p^5 4d\rightarrow 3p^5 4p$ transitions with the monochromator-PMT system and have found them to be of the order of 5% or less of the $3p^5 5s\rightarrow 3p^5 4p$ and $3p^5 3d\rightarrow 3p^5 4p$ cascades for all but the $2p_2$, $2p_3$, $2p_6$, $2p_9$, and $2p_{10}$ levels. At 20-eV energy and 3 mTorr, for example, $2p_2$ receives approximately 15% of its cascade from the $3p^5 4d$ and $3p^5 6s$ levels, $2p_3$ receives 16%, $2p_6$ receives 15%, $2p_9$ receives 21%, and $2p_{10}$ receives 13%. We include these cross sections in our total cascade measurements. For the remaining $2p$ levels we consider cascades only from the $3p^5 5s$ and $3p^5 3d$ levels, as any additional contributions are much smaller than the systematic uncertainty of our measurements.

C. Direct excitation cross sections

Once the total cascade cross sections are obtained, they can be subtracted from the apparent excitation cross sections, yielding direct excitation cross sections, as in Eq. (3). We list in Table II the measured emission cross sections at 40 eV and 1 mTorr for the cascades from the $2s$, $3d$, and $3s_1$ levels into the $2p$ levels. The uncertainties listed for the individual cross sections are purely statistical. The systematic uncertainty due to the inaccuracies in measuring the pressure, electron current, and wavelength response of the FTS is estimated to be 15%. In addition, there is a 12% systematic uncertainty due to error in the absolute cross section of the 912.3-nm line used for bridge calibration. The total cascades with quoted uncertainties including both statistical and systematic types are given in Table III. The small amounts of cascade from the $3p^5 6s$ and $3p^5 4d$ levels, though not listed in Table II, are taken into account in Table III. Also included in Table III are the apparent excitation cross sections for ten $2p$ levels at 40 eV and 1 mTorr and the direct excitation cross sections resulting from applying the cascade corrections. The uncertainties shown for both apparent and direct excitation cross sections include both the statistical and systematic types. Note that although the uncertainty on the apparent and cascade cross sections is relatively small (generally 20% or less), some of the direct cross sections show a much larger percentage of error. This effect arises because the direct cross section is the difference between two values of comparable magnitude. Since the errors add in quadrature, the uncertainty for the direct cross section can be proportionally much greater than the uncertainties on either the apparent or cascade cross sections.

Despite the pressure dependence of the observed emission cross sections illustrated in Fig. 4, the direct excitation cross

TABLE III. Total apparent, cascade, and direct cross sections at 40 eV and 1 mTorr in units of 10^{-19} cm^2. The direct cross sections are calculated by subtracting the total cascades of Table II from the apparent cross sections. Cascades for $2p_2$, $2p_3$, $2p_6$, $2p_9$, and $2p_{10}$ have additional contributions from $3s$ and $4d$ levels. Uncertainties are the combined systematic and statistical errors.

	$2p_1$ ($J=0$)	$2p_2$ ($J=1$)	$2p_3$ ($J=2$)	$2p_4$ ($J=1$)	$2p_5$ ($J=0$)	$2p_6$ ($J=2$)	$2p_7$ ($J=1$)	$2p_8$ ($J=2$)	$2p_9$ ($J=3$)	$2p_{10}$ ($J=1$)
Apparent	37±5	21±3	32±4	19±2	19±2	42±5	29±3	47±6	32±4	52±9
Cascade	6.3±1.5	12±2	16±3	10±2	6.7±1.6	20±5	15±3	20±4	26±3	28±3
Direct	31±5	9.1±3.7	16±5	9.0±3.2	12±3	22±7	14±5	27±7	6.1±4.9	24±11

sections for a given energy, determined at different pressures, are found to show little variation. Figure 5 shows apparent, cascade, and direct cross sections between 0.5 and 4 mTorr for the ten $2p$ levels at an incident electron energy of 100 eV. Therefore, within our experimental uncertainty, the observed pressure dependence of the $2p$ cross-section data can be attributed entirely to cascade, and there is no evidence of collisional excitation transfer into the $2p$ levels at pressures up to 4 mTorr. Direct excitation cross sections at 20, 40, and 100 eV obtained by averaging the results of measurements at 1, 2, and 3 mTorr are given in Table IV. The quoted uncertainty is the combined statistical and systematic errors.

Earlier works on electron excitation of rare-gas atoms from our laboratories indicated that at high energies, the cross sections for the $2p$ levels with even values of J are larger than those with odd J [4]. Based on group theoretical arguments it was shown that if we consider the Coulomb, but not the exchange, interactions between the incident electron and the argon atom, the direct coupling potential between the ground level ($3p^6\ ^1S_0$) and a $2p$ level of odd J value vanishes on account of rotational symmetry. However, the coupling is generally not equal to zero for a $2p$ level of even J. Since to first order the cross sections (neglecting projectile-target exchange interaction) are dictated by this coupling, we expect the cross sections for the $2p$ odd J levels to be smaller than the ones with even J. The cross sections given in Table IV generally conform to this trend at 100 eV. However, the $2p_7$ (J=1) appears to have a cross section comparable to $2p_3$ (J=2), $2p_5$ (J=0), and $2p_6$ (J=2). Unfortunately, the $2p_7$ cross section, $(11\pm5)\times10^{-19}$ cm^2, has the largest uncertainty. This, coupled with the uncertainties of the $2p_3$, $2p_5$, and $2p_6$ cross sections, does not make it possible at this time to establish clearly whether the $2p_7$ direct cross section is larger or smaller than the cross sections of these three even-J levels.

D. Origin of the pressure effects

We attribute the pressure dependence of the cascade cross sections to radiation trapping. A detailed theoretical treatment of the effect of radiation trapping on electron excitation experiments may be found elsewhere [5,13,14]. Here we discuss only qualitative aspects that are related to our experiments. Shown in Fig. 6 is a level a with $J=1$ that decays in an optically allowed transition not only to the ground level g (J=0), but also to a number of other levels $b,c,\ldots$, with $J=0$ or 2. Reabsorption of the $a\rightarrow g$ resonant radiation by a ground-level atom with the subsequent decay into level b results in a pressure-dependent effective branching ratio for the $a\rightarrow b$ transition and therefore a pressure-dependent emission cross section. Optical cross sections from such levels have long been known to show pressure dependence [14]. However, levels not optically connected to the ground level, such as the $3p^5 4p$ levels, can also display pressure dependence due to cascade from higher levels. For instance, although a $2p$ level with $J=0$, 1, or 2 is not optically coupled to the ground level (same parity), it may receive significant cascade from the $J=1$ levels of the $3p^5 4s$ and $3p^5 3d$ configurations which do decay to the ground level, so that the total population of this $2p$ level will be affected by reabsorption and display a dependence on pressure.

The $2p_9$ ($J=3$) level could also exhibit pressure dependence through a more complicated chain of events. The $3p^5 3d$ levels with $J=2$ which can cascade into the $2p_9$ are not themselves optically coupled to the ground level. However, they receive cascade from higher levels. For example, the radiatively trapped $3p^5 6s$ cascades to the $3p^5 5p$, which subsequently decays to the $3p^5 3d$ levels, giving them pressure dependence. This $3p^5 3d$ cascade then provides pressure dependence to the $2p_9$ level. However, the pressure dependence due to such a multiple cascade mechanism should be much weaker. At each step in the chain, the pressure-dependent cascade component is added to the pressure-independent direct excitation process, so that the pressure dependence is attenuated in each step. This is consistent with the weak pressure dependence for the $2p_9$ apparent cross section, as shown in Fig. 4. Furthermore, in Fig. 5 the cascade curve for $2p_9$ is flat at pressures below 1 mTorr, whereas the pressure dependence of the cascade for the other nine levels persists even at the lowest pressure point of 0.5 mTorr.

To illustrate further the effects of resonance radiation reabsorption, we plot in Fig. 7 optical emission cross sections at 100 eV versus pressure for the resonant $2s_4$ and $3d_2$ ($J=1$) and the nonresonant $2s_5$ and $3d_3$ ($J=2$) levels. It is clear from the figure that the $J=1$ levels, which experience radiation trapping, display a much larger variation with pressure than the $J=2$ levels, which acquire their pressure dependence through the smaller effect of cascades. We would therefore expect those $3p^5 4p$ levels receiving cascade predominantly from resonant levels to exhibit greater variation with pressure than those receiving more cascade from nonresonant levels. Figure 5 illustrates this. In the case of the $J=0$ levels, 100% of their cascade is from resonant levels, so they might be expected to show large pressure effects. However, their direct cross sections are large relative to their cascades. This tends to decrease the percentage effect of

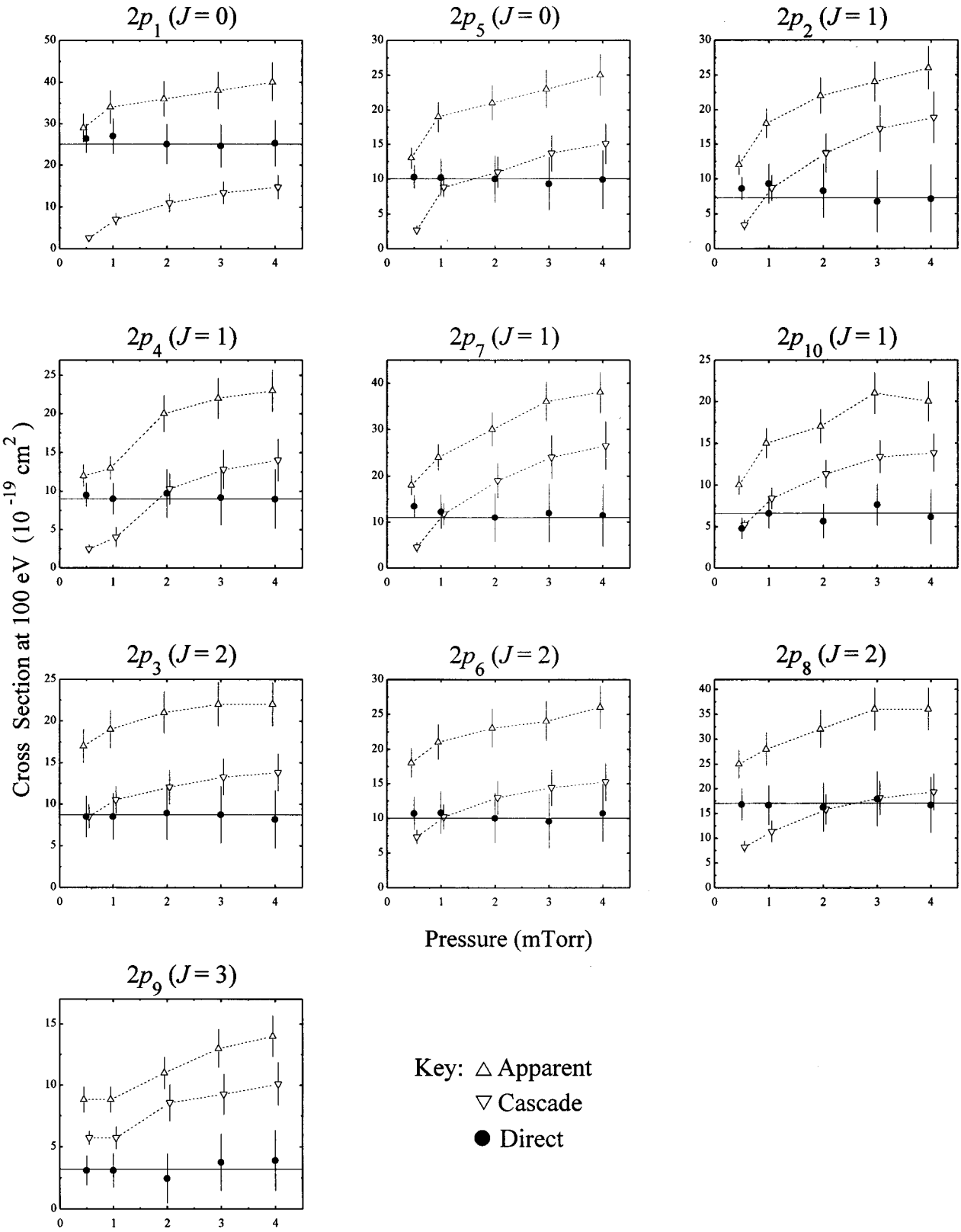

FIG. 5. Apparent (△), cascade (▽), and direct (●) cross sections versus pressure at 100 eV. Error bars are combined statistical and systematic. All data were taken at 0.5, 1, 2, 3, and 4 mTorr. Slight horizontal offsets have been added to the three data sets to make the points more easily readable.

pressure on their apparent cross sections. The $2p_2$, $2p_4$, and $2p_7$ $(J=1)$ levels receive, for example, approximately 90% of their cascade from resonant levels at 100 eV and 1 mTorr. For these levels, cascades make up a larger fraction of the apparent cross sections than they do for the $J=0$. This gives them the largest pressure effects of all the $2p$ levels. The $2p_{10}$ $(J=1)$ level differs somewhat from the other three $J=1$ levels in that only about 50% of its cascade comes from

TABLE IV. Direct cross sections for the $2p$ manifold of argon at various incident electron energies in units of 10^{-19} cm^2. These values represent the average of our measurements at 1, 2, and 3 mTorr. Quoted uncertainties are combined statistical and systematic errors.

Energy (eV)	$2p_1$	$2p_2$	$2p_3$	$2p_4$	$2p_5$	$2p_6$	$2p_7$	$2p_8$	$2p_9$	$2p_{10}$
20	50±7	14±6	29±9	22±7	16±4	32±12	25±9	54±15	53±22	47±22
40	31±5	9.0±4.5	17±6	9.0±3.7	14±4	19±7	13±6	26±8	6.3±5.0	25±10
100	25±5	6.8±3.9	8.7±3.3	9.0±3.1	10±3	10±4	11±5	17±5	3.1±2.0	6.6±2.5

the resonant levels. However, its direct excitation cross sections are likewise smaller than those of the other $J=1$ levels, so we see comparable pressure effects from all $J=1$ levels. The three $J=2$ levels each receive about 40% of their cascade from resonant levels (mostly $2s_2$ and $2s_4$) at 100 eV and 1 mTorr. Their cascade and direct cross sections are closer in magnitude than the other levels. Hence, these levels have suppressed pressure effects, in relation to the other $2p$ levels. Finally, in the case of the $2p_9$ ($J=3$) level, the cascade contribution is much larger than the direct. Despite the fact that it receives no resonant cascade, it still displays pressure effects due to the somewhat less pressure-dependent nonresonant cascades.

It is important to note that these pressure effects are dependent upon experimental geometry [5]. In this work, practical considerations forced us to place each detector system (monochromator-PMT and FTS) on different collision chambers. However, both the chambers and electron guns were of sufficiently similar design, so that pressure effects between the two chambers were identical. This was verified by examining on both systems cross section versus pressure curves for various lines originating from the same $2p$ level. In all cases the curves were identical.

E. Shape of the excitation functions

The apparent, total cascade, and direct excitation functions for all ten $2p$ levels at 3 mTorr are shown in Fig. 8. These plots demonstrate the important role cascade processes play in populating the $2p$ levels. In the case of the $J=1$ and $J=3$ levels at 3 mTorr, cascade contributions are greater than direct excitation over nearly the whole energy range. For the $J=2$ levels and the $2p_5$ level ($J=0$), cascade cross sections are comparable to the direct cross sections. Only in the case of $2p_1$ ($J=0$) do we find the direct excitation cross section dominating the cascade over the entire energy range. The effect of the cascade is to exaggerate the height of the high-energy tail, relative to the peak, of the excitation function.

Cascade contributions can have great effects on the shapes of the excitation functions. In the case of the two $J=0$ levels, the cascade is responsible for creating the ''double peak'' shape of the apparent excitation function, which has been observed by other investigators [4,15]. Cascade into the $J=0$ levels comes only from the $J=1$ levels of the $3p^5ns$ and $3p^5nd$ configurations, which tend to have characteristically broad shapes, peaking between 60 and 100 eV [4]. This, combined with the direct excitation, which peaks around 20 eV, creates the multiple peaks. As pressure increases, the strongly pressure-dependent cascade increases, and the high-energy peak is enhanced.

As shown previously in Fig. 4, the $2p$ apparent cross sections display greater pressure dependence at higher incident electron energies. From Fig. 8 we can see the reason for this in the following way. At high energies the cascade curve is dominated by the broad shapes that can be associated with the cascading lines from the $J=1$ levels of the $3p^5ns$ and $3p^5nd$ configurations, because these levels are optically

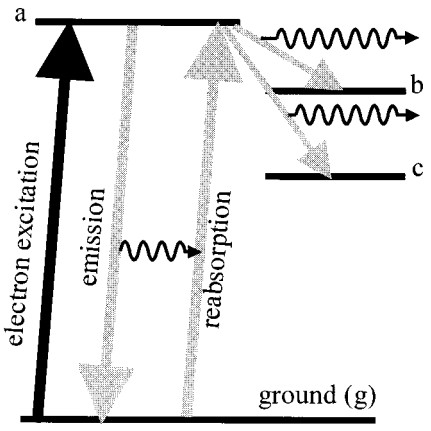

FIG. 6. Resonant radiation reabsorption. Level a is optically coupled to the ground level (g), while b and c are not. Photons emitted in the $a \rightarrow g$ transition reexcite atoms back to level a, giving them a ''second chance'' to radiate to b or c. The result is a pressure-dependent branching ratio with $a \rightarrow g$ tending to zero at high pressure.

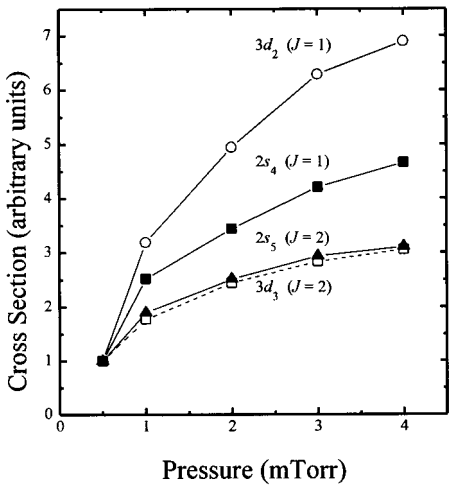

FIG. 7. Cross section vs pressure for two $J=1$ resonant (○ and ■) and two $J=2$ nonresonant (▲ and □) cascade transitions. The cross sections have all been normalized to 1 at 0.5 mTorr. Error bars have been omitted for clarity, but would be approximately 5%.

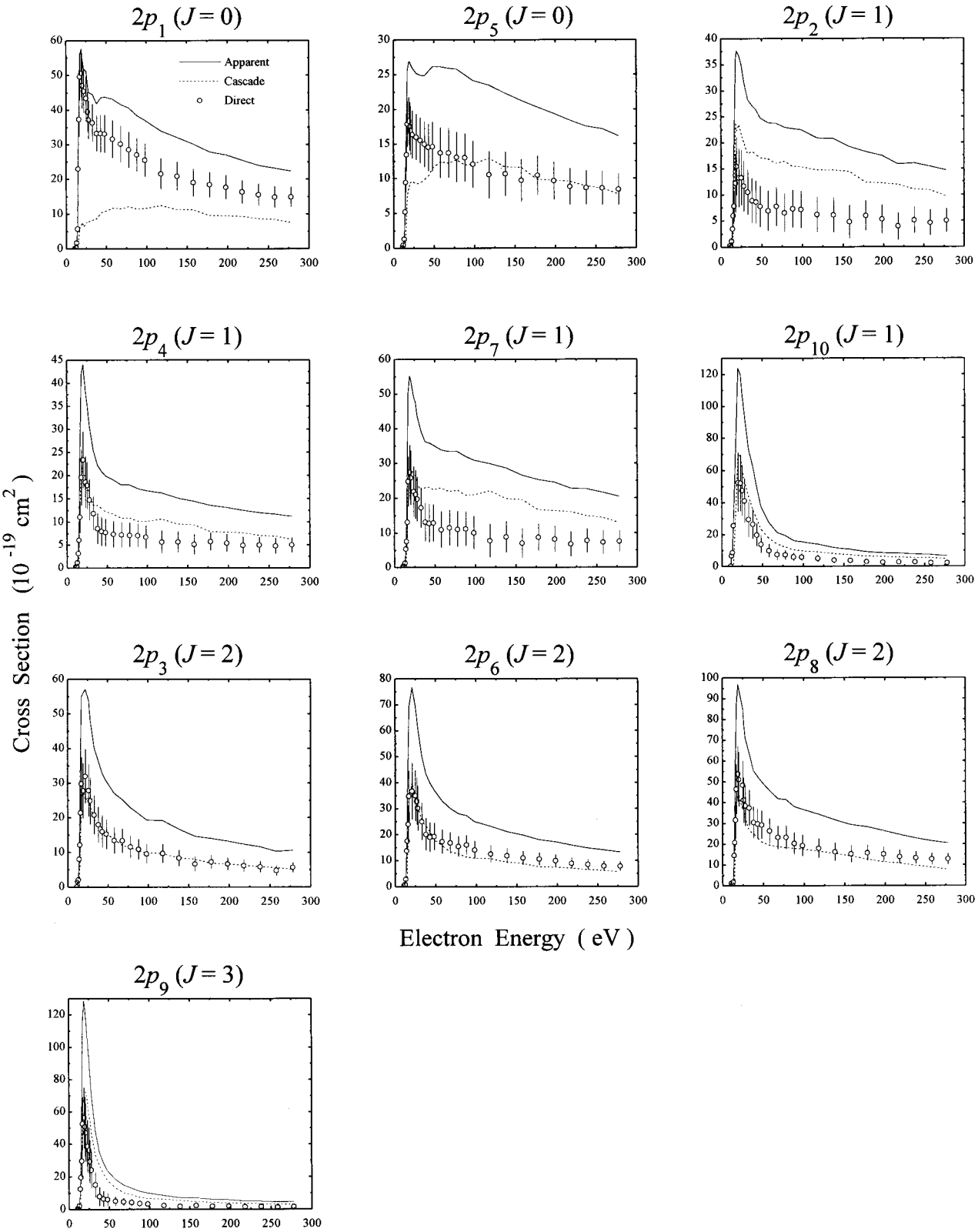

FIG. 8. Excitation functions for apparent (solid curve), cascade (dashed curve), and direct (circles) cross sections of the $2p$ manifold at 3 mTorr. Error bars have been omitted from the apparent and cascade measurements for clarity. Those on the direct cross sections are combined statistical and systematic.

coupled to the ground level with, in most cases, a very broad excitation function peaking around 60–100 eV, as shown in Ref. [4]. The extreme pressure effect of these cascading lines manifests itself through radiation trapping as the more exaggerated pressure dependence of the apparent cross sections at 100 eV, as compared to 20 eV.

The very sharp direct excitation function for the $2p_9$ $(J=3)$ is well understood on the grounds that it is the only

TABLE V. Comparison of our $2p$ apparent cross sections extrapolated to zero pressure with those of Ref. [15], for 100-eV incident energy. Cross sections are in units of 10^{-19} cm^2.

	$2p_1$	$2p_2$	$2p_3$	$2p_4$	$2p_5$	$2p_6$	$2p_7$	$2p_8$	$2p_9$
This work	25±5	6.8±1.3	17±5	9.0±1.8	10±2	18±5	11±2	23±7	7.6±2.3
Ref. [15]	22±3	6.1±1.1	14±3	4.8±1.6	8.1±1.2	16±3	8.3±2.4	22±6	8.4±2.8

state in the $3p^5 4p$ configuration with $J=3$, and is a pure L-S coupled state. If we use the intermediate-coupling scheme to write the wave functions for the levels as linear combinations of L-S terms of the same J from the $3p^5 4p$ configuration, the $2p_9$ wave function is represented solely by the $3p^5 4p(^3D_3)$ term, so that the excitation function is expected to have the sharp peak characteristic of a spin changing excitation ($^1S \rightarrow {}^3L$) [16]. The similar sharp peak in the $2p_{10}$ data can also be explained in terms of its wave function. The $2p_{10}$ state ($J=1$) is a superposition of the L-S eigenfunctions for $^3S_1$, $^3P_1$, $^3D_1$, and $^1P_1$. The g factors for these L-S eigenfunctions are 2.0, 1.5, 0.5, and 1.0 respectively. The $2p_{10}$ level has a g factor of 1.985 [17]. Therefore its wave function is dominated by the $^3S_1$ term with only a small amount of singlet admixture, hence the sharp peak in the excitation function.

For excitation from a singlet into a triplet level, the excitation function is expected to show an E^{-3} dependence at high energies according to the Born-Ochkur theory. It should be interesting to check whether this inverse cubic relation is reflected in our $2p_9$ results. However, as can be seen in Fig. 8, for the $2p_9$ level the apparent excitation cross sections are only slightly larger than the cascade, so that the direct excitation cross sections obtained from their differences are not accurate enough for a quantitative test of the energy dependence. Qualitatively, however, both the $2p_9$ and $2p_{10}$ direct excitation functions display a greater falloff with energy than the other $2p$ levels.

F. Comparison with previous results

Tsurubuchi *et al.* [15] recently published apparent excitation cross sections for nine of the ten $2p$ levels but gave no cascade or direct excitation cross sections. They observed a similar pressure dependence of the optical emission cross sections. By extrapolating our $2p$ apparent cross sections to the zero-pressure regime, we see a good agreement between the two experiments, as illustrated in Table V. Ballou *et al.* [4] also measured the apparent $2p$ cross sections. Most of their measurements were done at pressures above 1 mTorr. Thus their apparent cross sections are probably not free from pressure effects and do not correspond to the values at the limiting zero pressure regime of Table V.

Two other works have reported attempts at measuring the direct $2p$ cross sections. Bogdanova and Yurgenson [18] used a pulsed electron beam to reduce cascade transitions in order to measure direct cross sections for the $2p$ levels. Their direct excitation cross sections are generally in good agreement with ours, as shown in Table VI.

Chutjian and Cartwright [19] performed energy-loss measurements of electron impact on argon, and tabulated differential excitation cross sections for scattering angles between 10° and 140°. By extrapolating the differential cross sections to the unmeasured angles and integrating over all scattering angles, (integrated) direct excitation cross sections may be obtained. We compare their results of $2p$ direct excitation cross sections to ours in Table VI. For most of the levels, agreement between the two experiments is poor, with their values smaller than ours. Determination of (integrated) direct excitation cross sections by measurement of differential cross sections is complicated by the necessity of extrapolation to the small- and large-angle regions.

V. CONCLUDING REMARKS

Use of the FTS in conjunction with monochromator-PMT detection enables an extensive analysis of electron-impact excitation of the $2p$ levels of argon using the optical method. As in earlier works, the apparent excitation cross sections are obtained by measuring the emission intensities of all transitions from the $2p$ levels in the wavelength range of 660–1150 nm. In the past it was difficult to extract the direct excitation cross sections from these optical measurements because the major cascading radiation into the $2p$ levels are in the IR (1150–1600 nm) outside the detection range of the PMT. The FTS technique makes it possible to measure the

TABLE VI. Comparison of our $2p$ direct cross sections with those of Refs. [18] and [19] at the peak and at 100-eV incident energy, extrapolated to zero pressure. Cross sections are in units of 10^{-19} cm^2.

	$2p_1$	$2p_2$	$2p_3$	$2p_4$	$2p_5$	$2p_6$	$2p_7$	$2p_8$	$2p_9$	$2p_{10}$
					Peak cross sections					
This work	50±7	14±6	29±9	22±7	16±4	32±12	25±9	54±15	53±22	47±22
Ref. [18]	52±16	18±5	37±11	17±5	16±5	17±5	19±6	24±7	39±12	
Ref. [19]	27±8	5.8±2.7	11±5			15±5	14±5	13±4	24±8	14±4
					Cross sections at 100 eV					
This work	25±5	6.8±3.9	8.7±3.3	9.0±3.1	10±3	10±4	11±5	17±5	3.1±2.0	6.6±2.5
Ref. [18]	30±9	8.2±2.5	15±4	5.3±1.6	12±4	10±3	11±3	8.8±2.6	3.7±1.1	
Ref. [19]	18±5	0.95±0.45	5.0±2.4			5.9±1.9	1.9±0.9	6.7±2.2	0.93±0.44	0.54±0.25

cascade radiation and to obtain the direct excitation cross sections of the $2p$ levels by optical measurements.

Earlier experiments [3] reported pressure dependence of the measured shape of the $2p$ apparent excitation functions and the magnitude of the apparent cross sections at pressures as low as a few mTorr. Our FTS measurements for the IR lines cascading into the $2p$ levels also show pressure dependence. However, when the total cascades are subtracted from the apparent excitation cross sections, the resulting direct excitation cross sections are independent of the pressure within experimental uncertainty. The pressure dependence of the cascading radiation is attributed to radiation trapping, which makes the population of the optically allowed levels (with respect to the ground level) dependent on pressure, and this pressure effect propagates to the lower levels through spontaneous emission.

When the cascade constitutes a large fraction of the apparent excitation cross section, the percentage error of the direct excitation cross section becomes much larger than that of the apparent excitation cross section. Thus, in Table IV, we see uncertainties as large as $\sim 50\%$ for the direct excitation cross sections at 100 eV (even larger for the $2p_9$ level). This problem is accentuated by the necessity of measuring the apparent excitation cross sections with one apparatus (monochromator-PMT), and the cascade with another (FTS), so that the resulting direct excitation cross sections are subject to two sets of systematic uncertainties. A possible improvement is to incorporate both the monochromator-PMT and the FTS detection systems on the same collision chamber. This would allow measurements of apparent and cascade cross sections to be made at exactly the same conditions so as to reduce the uncertainty arising from taking the difference between the apparent and cascade cross sections.

Determination of cascade is a central task in the optical method for measuring electron-impact excitation cross sections. For a few cases, a full account of the cascade can be made from experiments in the visible region so that accurate direct excitation cross sections can be obtained from the measured apparent cross sections [6]. However, in most cases, many of the cascade transitions are in the IR and cannot be measured by conventional PMT detection. This indeed has been a major impediment in using the optical method to determine direct excitation cross sections. The incorporation of the FTS technique in the electron excitation experiment represents a significant advance toward solving the problem of cascade measurement. This is well demonstrated in our work on argon reported here, and extension to other atoms can be similarly made. An important effort in the future is to improve the accuracy of the individual optical measurements, since the direct excitation cross section is the difference between two measured quantities often of comparable magnitude. Also, development of more sensitive detection techniques in the far infrared region is most desirable. Finally, it should be mentioned that in addition to cascade measurements, the FTS technique also enables one to study excitation of energy levels that radiate only in the IR such as the $5d$ levels of Xe, shown in the pioneering work of DeJoseph and Clark [1].

ACKNOWLEDGMENTS

The authors wish to express their deep appreciation to Dr. Charles A. DeJoseph for his expert advice on the FTS techniques, which has been most instrumental in making this work possible. They also acknowledge Mark Lagus for his electron gun construction. This work was supported by the United States Air Force Office of Scientific Research.

[1] C. A. DeJoseph, Jr. and J. D. Clark, J. Phys. B **23**, 1879 (1990).
[2] See, for example, J. W. McConkey and F. G. Donaldson, Can. J. Phys. **51**, 914 (1973); J. M. Ajello, G. K. James, B. Franklin, and S. Howell, J. Phys. B **23**, 4355 (1990).
[3] R. S. Schappe, M. B. Schulman, L. W. Anderson, and C. C. Lin, Phys. Rev. A **50**, 444 (1994).
[4] J. K. Ballou, C. C. Lin, and F. E. Fajen, Phys. Rev. A **8**, 1797 (1973).
[5] A. H. Gabriel and D. W. O. Heddle, Proc. R. Soc. London, Ser. A **258**, 124 (1960).
[6] A. R. Filippelli, C. C. Lin, L. W. Anderson, and J. W. McConkey, Adv. At., Mol., Opt. Phys. **33**, 1 (1994).
[7] B. L. Moiseiwitsch and S. J. Smith, Rev. Mod. Phys. **40**, 238 (1968).
[8] P. R. Griffiths and J. A. de Haseth, *Fourier Transform Infrared Spectrometry* (John Wiley & Sons, New York, 1986).
[9] A. R. Filippelli, S. Chung, and C. C. Lin, Phys. Rev. A **29**, 1709 (1984).
[10] W. L. Wiese, J. W. Brault, K. Danzmann, V. Helbig, and M. Kock, Phys. Rev. A **39**, 2461 (1989).
[11] W. L. Wiese, M. W. Smith, and B. M. Miles, *Atomic Transition Probabilities*, Natl. Bur. Stand. (US), Nat. Stand. Ref. Data. Ser. No. 22 (U.S. GPO, Washington, D.C., 1969), Vol. II.
[12] W. Whaling, M. T. Carle, and M. L. Pitt, J. Quant. Spectrosc. Radiat. Transf. **50**, 7 (1993).
[13] D. W. O. Heddle, Adv. At. Mol. Phys. **15**, 381 (1979).
[14] A. V. Phelps, Phys. Rev. **110**, 1362 (1958).
[15] S. Tsurubuchi, T. Miyazaki, and K. Motohashi, J. Phys. B **29**, 1785 (1996).
[16] C. C. Lin and L. W. Anderson, Adv. At., Mol., Opt. Phys. **29**, 1 (1991).
[17] C. E. Moore, *Atomic Energy Levels Vol. 1*, National Bureau of Standards Circular No. 467 (U.S. GPO, Washington, D.C., 1949), p. 212.
[18] I. P. Bogdanova and S. V. Yurgenson, Opt. Spectrosk. **62**, 471 (1987) [Opt. Spectrosc. USSR **62**, 281 (1987)].
[19] A. Chutjian and D. C. Cartwright, Phys. Rev. A **23**, 2178 (1981).